Polímeros
ISSN 1678-5169 (Online)

https://doi.org/10.1590/0104-1428.20220121

ORIGINAL ARTICLE

# Evaluation of potential biomaterials for application in guide bone regeneration from Bacterial Nanocellulose/Hydroxyapatite

**Elouise Gaulke[1], Michele Cristina Formolo Garcia[2,3]*, Bruna Segat[2], Giannini Pasiznick Apati[2], Andréa Lima dos Santos Schneider[2,3], Ana Paula Testa Pezzin[1], Karina Cesca[4] and Luismar Marques Porto[4]**

*[1]Laboratório de Materiais, Programa de Pós-graduação em Engenharia de Processos, Universidade da Região de Joinville, Joinville, SC, Brasil*

*[2]Laboratório de Biotecnologia I, Departamento de Engenharia Química, Universidade da Região de Joinville, Joinville, SC, Brasil*

*[3]Laboratório de Biotecnologia I, Programa de Pós-graduação em Saúde e Meio Ambiente, Universidade da Região de Joinville, Joinville, SC, Brasil*

*[4]Laboratório de Engenharia Biológica, Programa de Pós-graduação em Engenharia Química, Universidade Federal de Santa Catarina, Florianópolis, SC, Brasil*

**micheleformologarcia@gmail.com*

## Abstract

Bacterial nanocellulose (BNC) membranes have interconnected porous nanostructures and excellent biocompatibility. Functionalizing these with calcium phosphate sources and metal ions confers optimized properties to the biomaterial. This study aims to synthesize BNC membranes, functionalize them with copper and magnesium apatites, characterize and evaluate their cytotoxicity and antimicrobial potential. Membranes were synthesized for 8 days in Mannitol Medium. The biocomposite production was by immersion cycles. The biocomposites were characterized by porosity and swelling capacity, Fourier transforms infrared spectroscopy (FTIR), scanning electron microscopy (SEM), thermogravimetric analysis (TGA), antimicrobial properties and cytotoxicity assays. The FTIR and SEM results showed that phosphate groups were incorporated into the BNC. The TGA analysis also indicated the incorporation of the inorganic phase. The membrane functionalization with Cu promoted the antimicrobial properties of the biomaterial. However, functionalization with Mg had a more positive behavior on cell viability, proving to be more suitable for use as an implantable material.

**Keywords:** *apatites, bacterial nanocellulose, biocomposites, osteogenesis.*

**How to cite:** Gaulke, E., Garcia, M. C. F., Segat, B., Apati, G. P., Schneider, A. L. S., Pezzin, A. P. T., Cesca, K., & Porto, L. M. (2023). Evaluation of potential biomaterials for application in guide bone regeneration from Bacterial nanocellulose/Hydroxyapatite. *Polímeros: Ciência e Tecnologia*, *33*(3), e20230034. https://doi.org/10.1590/0104-1428.20220121

## 1. Introduction

The healing process of bone fractures is considered a regenerative and biologically complex process[1]. Autologous bone grafts have been pointed out as the primary solution[2]. However, there is still the risk of transmitting infectious diseases and rejection[3]. In this context, guided bone regeneration (GBR) appears as one of the most effective and reliable methods to promote bone restructuring[4]. In this context, scaffolds for bone regeneration emerged to mimic the natural extracellular matrix of bone (ECM), providing a basic structure and microenvironment for the growth of bone tissue with excellent biocompatibility, adaptable biodegradability, osteoconductivity and minimal immunogenic responses[5]. For this reason, different biomaterials have been studied.

BNC is an extracellular polysaccharide produced by some bacterial genera, especially the species of *Komagataeibacter*[6]. Its surface allows the adsorption of metallic ions or metallic nanoparticles[7]. It has low rejection and inflammatory reaction due to its excellent biocompatibility, good permeability, hygroscopicity, and flexibility, allowing its wide use in tissue engineering as a scaffold[8]. However, BNC alone does not have all the properties necessary to act as a device for a bone implant.

In this context, the incorporation of hydroxyapatite (HAp) in the BNC matrix[9] is studied. The chemical similarity of HAp to the naturally occurring bone matrix, biocompatibility, non-toxicity and high osteoconductivity makes it highly attractive for bone regeneration and implantation[10].

The biocomposite of BNC/HAp is formed by the porous membrane reinforced with HAp crystals. This structure allows this material to trigger the fixation and proliferation of bone cells at the defect site[9]. In addition, since the HAp particles are physically attached to the BNC fibers, these particles do not migrate to neighboring areas, preventing damage that could be caused to the surrounding soft tissues[4,10]. Furthermore, adding divalent cations to these biomaterials can promote optimized characteristics.

Copper (Cu) is an essential micronutrient involved in the immune system and has bacteriostatic and antibacterial effects, modifying cell permeability and eventually leading to bacterial cell death[11]. In addition, it has the potential to stimulate angiogenic properties, assist in the regulation of bone resorption rate and increase the deposition of collagen fibers, attributing several functionalities when incorporated into HAp[11].

Magnesium (Mg) is also an essential trace element; it acts in bone resorption processes and stimulates the proliferation of osteoblasts[12]. The degradation product ($Mg^{2+}$) is a standard human body composition with antitumor and antibacterial characteristics, reducing the risk of infections and the need for further surgeries[13]. Combined with natural calcium phosphate, it helps the spontaneous formation of bone bonding in vivo[14], which can alter the mineral metabolism, resulting in the modification of the dissolution rate of the crystals and the biodegradation of the related materials[15].

In this context, this work aimed to synthesize and characterize BNC membranes functionalized with copper and magnesium apatites, seeking to produce a biocomposite for application in GBR and evaluate its antimicrobial activity and cytotoxicity. The study stands out because it aims at combining biomaterials that have the potential to mimic the native bone structure and the extracellular matrix. Furthermore, including bivalent cations found in bone tissue may increase the osteogenic potential, optimizing the synergistic effects of this biomaterial.

## 2. Materials and Methods

### 2.1 Biosynthesis and purification of BNC membranes

For this, the bacterium *Komagataeibacter hansenii* ATCC 23769 was used. The culture medium used in the cell activation step and the production of membranes was the Mannitol Medium (MM) (pH 7), consisting of (g $L^{-1}$): 20 g mannitol, 5 g peptone, 5 g yeast extract. In the cell activation step, one Eppendorf tube containing the microorganism was added to an Erlenmeyer flask and incubated at 30 °C under static conditions for two days. Then, this pre-inoculum was transferred to the culture medium at a rate of 20% (v/v), containing an optical density between 0.15 and 0.19, measured by absorbance in a spectrophotometer at 600 nm. The culture medium was incubated at 30 °C under static condition for 8 days to form of BNC membranes. The formed membranes were removed from the surface of the liquid culture, washed with water, and treated with a 0.1 M NaOH solution at 80 °C for 60 min. After that, the membranes were washed with distilled water until reaching pH 7, sterilized, and stored in a refrigerator, for later production of biocomposites.

### 2.2 Production of biocomposites

The biocomposites functionalized with Mg and Cu were produced according to the methodology described by Hutchens et al.[16]. The wet BNC membranes (never dried) were immersed in hybrid solutions of $MgCl_2$ (0.1 M) and $CaCl_2$ (0.1 M) or $CuCl_2$ (0.1 M) and $CaCl_2$ (0.1 M), with a pH between 4 and 5, in different proportions for 24 h under orbital agitation at 26 °C and 85 RPM. The concentrations of the tested solutions were 50% $CuCl_2$ or $MgCl_2$ and 50% $CaCl_2$, 30% $CuCl_2$ or $MgCl_2$ and 70% $CaCl_2$, and 10% $CuCl_2$ or $MgCl_2$ and 90% $CaCl_2$ concerning the $Na_2HPO_4$ solution (0.06 M) with pH 8. Subsequently, the membranes were washed with distilled water to remove residues from the previous step and immersed in a $Na_2HPO_4$ 0.06 M solution for another 24 h. Three immersion cycles were performed in each solution. The biocomposites formed were named BNC/MgHAp and BNC/CuHAp. Then, the biocomposites were lyophilized for 24 h and then characterized.

### 2.3 Characterization techniques

#### 2.3.1 Determination of porosity and swelling degree

The samples were weighed previously wet and after drying by lyophilization for 24 h. The porosity of biocomposites was determined according to the Equation 1[17].

$$\varepsilon(\%) = \frac{\frac{(m_1 - m_2)}{\rho_{water}}}{v} \times 100 \quad (1)$$

Where ε is the porosity of the membrane, $m_1$ and $m_2$ are the masses (g) of the wet and dry membrane, respectively, $\rho_{water}$ is the specific mass of water obtained at 20 ºC, which is equivalent to 0.9982 g/$cm^3$, and v is the volume ($cm^3$) calculated based on the membrane form.

For the determination of the swelling capacity of the biomaterials, the samples were immersed in distilled water until the sample mass remained constant (~1h). After immersion, excess water from the samples was removed with absorbent paper, and the samples were weighed. The degree of swelling was calculated according to Equation 2:

$$\%I = \frac{(m_1 - m_2)}{m_2} \times 100 \quad (2)$$

The samples were analyzed in triplicate and submitted to analysis of variance (ANOVA) using the OriginPro® 8.5 software.

#### 2.3.2 Fourier Transform Infrared Spectroscopy (FTIR)

Thirty-two scans were performed per sample from 4000 to 500 $cm^{-1}$, resolution of 4 $cm^{-1}$, using the attenuated total reflectance module (ATR) in a spectrometer (Perkin-Elmer).

#### 2.3.3 Scanning Electron Microscopy (SEM)

The samples were fixed on metallic supports and covered with gold. The equipment used was a SEM (JEOL, model JSM-6390LV). An electron beam bombarded the samples, and the X-rays emitted from the samples were detected by a silicon solid-state detector device for a point elemental analysis (EDS) of the sample.

#### 2.3.4 Thermogravimetric Analysis (TGA)

The TG and DTG curves were obtained using the TGA-Q50/TA Instruments. The samples were heated from 25 to 600 °C at a 10 °C/min rate under an oxidizing atmosphere.

### *2.4 Antimicrobial properties assay*

The antimicrobial properties assay was performed using the disk diffusion technique of Bauer et al.[18], using Müeller Hinton medium (MH) with the microorganisms *Escherichia coli* (ATCC 8739) and *Staphylococcus aureus* (ATCC 25923) activated for 24 h at 37 ºC, in Brain Heart Infusion Broth (BHI). The Mac Farland scale was used as a parameter of cell concentration of the evaluated microorganisms, standardizing the absorbance at 0.28 (according to the 0.5 tube of the Mac Farland scale). Then, disks (Ø 6 mm) of the biocomposites produced and a disk of pure BNC (BR), added to each plate as a control, were placed on the inoculated cells and incubated at 37°C for 24 h. The analysis was carried out in duplicate.

### *2.5 Cytotoxicity analysis*

Cytotoxicity analysis was evaluated by measuring the metabolic activity of mouse fibroblasts (line - L929) multiplied in Dulbecco's Modified Eagle's Medium (DMEM) supplied with 15% FBS, following ISO 10993-5[19], using the MTS colorimetric method[20]. The test was conducted in triplicate, and submitted to analysis of variance (ANOVA) using the OriginPro® 8.5 software.

## 3. Results and Discussions

### *3.1 Synthesis of the BNC membrane*

The BNC membrane formed after cultivating had a thickness varying between 2 and 3.5 mm (Figure 1A). After purification, the membranes had a gelatinous appearance in the form of a translucent hydrogel (Figure 1B). On the other hand, lyophilization brought a spongy characteristic to the membrane (Figure 1C).

### *3.2 Production of biocomposites*

The biocomposites formed showed a change in their color according to the percentage of the incorporated element (Mg or Cu) (Figure 2). The biocomposites obtained were lyophilized to maintain the pores' integrity and provide an environment conducive to the migration and cell adhesion of this material when implanted. According to Kim et al. [21], how bigger the porosity, the better the permeability of the material, which will facilitate vascularization, its gas exchange and the transport of nutrients to the cells, thus increasing the possibility of successful tissue regeneration.

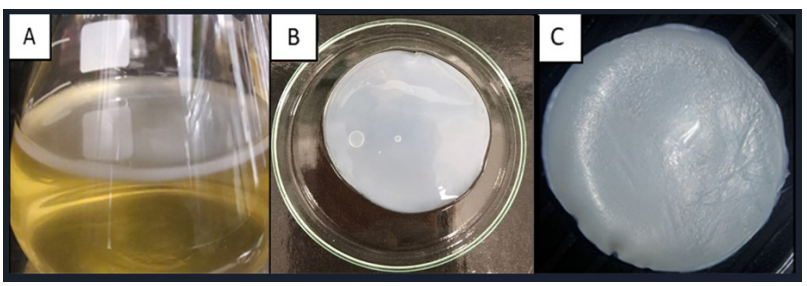


**Figure 1.** BNC membranes: (A) biosynthesis; (B) after purification; (C) after lyophilization.

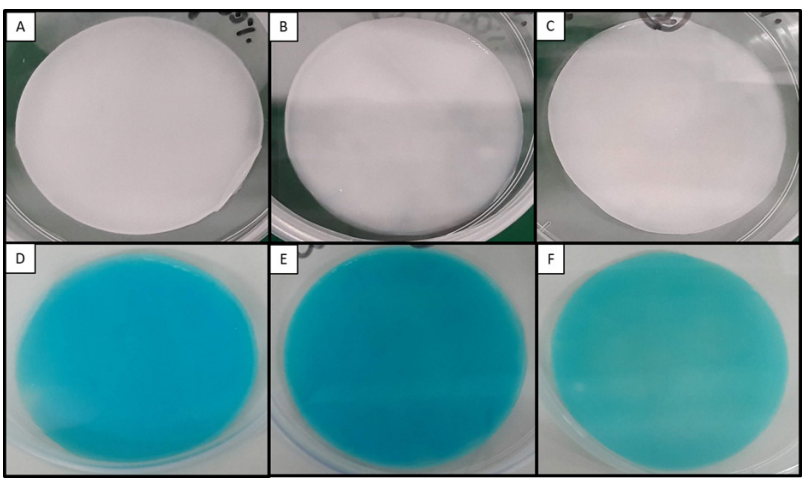


**Figure 2.** Biocomposites with different concentrations: (A) BNC/MgHAp 50%; (B) BNC/MgHAp 30%; (C) BNC/MgHAp 10%; (D) BNC/CuHAp 50%; (E) BNC/CuHAp 30%; (F) BNC/CuHAp 10%.

### 3.3 Characterization techniques

#### 3.3.1 Determination of porosity and swelling degree

BNC has a highly porous structure (96%), and incorporating inorganic material can affect this characteristic. According to Jin et al.[22], the pore size of the matrix decreases with increasing hydroxyapatite mass, and eventually, accumulations may occur in the pore structure.

The concentration of metal ions did not significantly influence the porosity values. However, Figures 3A and 3B show an average reduction of 15% in the average porosity percentage of the biocomposites concerning BNC, suggesting the deposition of inorganic material. This result suggests that metallic apatite deposition occurred superficially and inside the BNC. The biocomposites still maintained a high percentage of average porosity (± 80%). This characteristic is essential for implantable biomaterials because it helps anchor cells and distributes nutrients and growth or differentiation factors to cells.

The swelling of nanofibers is a fundamental parameter for biomaterials since they are designed to be used in high humidity conditions[23]. BNC showed significantly greater swelling capacity than functionalized biomaterials (Table 1). However, within the group of functionalized membranes, there was no significant difference in the samples' water absorption capacity, demonstrating that the partial replacement of $Ca^{2+}$ ions by $Mg^{2+}$ or $Cu^{2+}$ did not result in significant changes in this property in the biomaterials. This result is likely due to the similarities between these ions, such as similar ionic radius ($Ca^{2+}$ = 99 pm, $Mg^{2+}$ = 72 pm and $Cu^{2+}$ = 73 pm)[24] and the same valence ($^{2+}$). Thus, despite the decreased water absorption capacity, the biomaterials did not lose their swelling capacity and were as quick to absorb as pure BNC.

#### 3.3.2 Fourier Transform Infrared Spectroscopy (FTIR)

The FTIR spectrum (Figure 4) characteristic of pure BNC is marked by bands in the region of 3345 $cm^{-1}$, which according to He et al.[25], is characteristic of the stretching of the hydroxyl groups present in BNC. In addition, the CH stretching and asymmetric stretching at 2897 $cm^{-1}$, $CH_2$ deformation at 1427 $cm^{-1}$, OH deformation at 1315 and 1359 $cm^{-1}$, as well as the antisymmetric bridge of the C-O-C stretch at 1109 and 1162 $cm^{-1}$ and the band in the region of 1056 $cm^{-1}$ related to the vibrations of the C-O stretch are characteristic of BNC[26,27]. Another exciting band, located around 400 to 700 $cm^{-1}$, is characteristic of the torsion of the OH groups.

However, it is worth mentioning that typical HAp behaviors are also observed in the composites; this can be verified in the band around 1248 $cm^{-1}$, which, according to Salarian et al.[28], can be attributed to the P–O stretching vibration of $PO_4^{3-}$, the band at 1367 $cm^{-1}$ was also attributed by Panda et al.[29] to the presence of carbonate ions in a Ca-deficient HAp, indicating cationic substitution in the biocomposites produced in this work. Another point worthy of note is the band at 3345 $cm^{-1}$, attributed to the BNC hydroxyls, which had its intensity significantly reduced in the biocomposite spectra. According to Minatti[30], this change in intensity suggests that the HAp crystals affected the hydroxyl groups of the BNC, confirming an interaction between the OH group and the HAp. The chemical interaction between BNC and HAp stabilizes the biocomposite to maintain mechanical integrity.

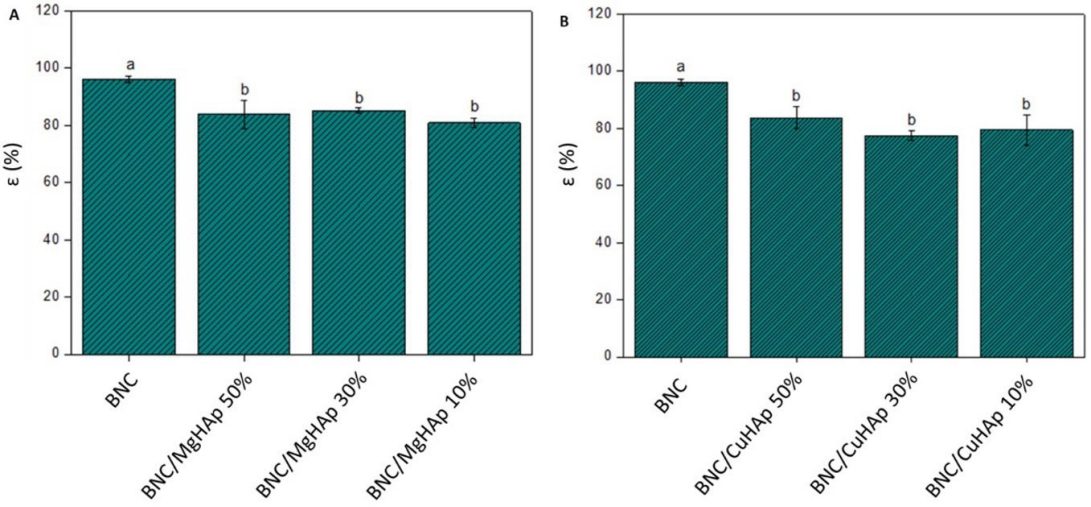


**Figure 3.** Analysis of the average percentage of porosity: (A) BNC/MgHAp; (B) BNC/CuHAp.

**Table 1.** Study the degree of water absorption by samples of BNC and functionalized biomaterials.

| Samples | BNC | BNC/ MgHAp50% | BNC/ MgHAp30% | BNC/ MgHAp10% | BNC/ CuHAp50% | BNC/ CuHAp30% | BNC/ CuHAp10% |
|---|---|---|---|---|---|---|---|
| Swelling capacity (%) | 629.3 ± 56.44[a] | 304.9 ± 19.82[b] | 251.6 ± 27.59[b] | 218.7 ± 0.45[b] | 251.6 ± 6.17[b] | 266.1 ± 18.92[b] | 263.9 ± 35.41[b] |

Lowercase letters indicate comparisons between the biocomposites and the BNC (control). Equal letters indicate means that did not differ from each other.

The bands at 1030 $cm^{-1}$ and 962 $cm^{-1}$, are related to the $PO_4$[31,32]. The band at 1030 $cm^{-1}$ was observed only for the samples BNC/CuHAp30% and BNC/MgHAp10%, while the bands at 962 $cm^{-1}$ were seen in all analyzed samples (Figure 4). According to Hutchens et al.[16], these two bands may represent the elongation mode of the phosphate group vibration, which can overlap the BNC membrane groups at wavenumbers between 1000 and 1100 $cm^{-1}$.

Bands at 1750 and 873 $cm^{-1}$ were also observed in all functionalized biomaterials, corresponding to the C=O bond and the carbonate ion ($CO_3^{-2}$), indicating that part of the phosphate group incorporated into the BNC was replaced by carbonate. This replacement can be attributed to the $CO_2$ present in the air since the functionalization was produced under agitation. Wan et al.[33] highlighted that the composition and structure of the incorporated carbonate produce an apatite similar to that found in natural bone.

### 3.3.3 Thermogravimetric Analysis (TGA)

Figure 5 shows the TG and DTG curves obtained for BNC, Mg, and Cu apatites. Pure BNC presented the first stage of mass loss of 1.77%, (Table S1), which refers to the water loss present in the sample. The second stage occurred at $T_{peak3}$ at 316 ºC, where the highest percentage of sample mass loss was observed, equivalent to 74.38%, related to cellulose degradation. The last stage of degradation for the BNC showed a mass loss of 17.19%, which occurred at $T_{peak4}$ of 494 ºC and is related to the degradation of carbonaceous residues[34].

The BNC/MgHAp50%, BNC/MgHAp30%, BNC/MgHAp10% and BNC/CuHAp10% samples showed an additional mass loss stage of 6.6%, 7.1%, 1.6% and 2.0%, respectively, with $T_{peak2}$ around 180 ºC. This event can be attributed to adsorbed water in HAp that is reversibly removed from 25 to 200 °C without affecting the network parameters[35].

The $T_{peak3}$ presented by BNC was 316 ºC, while for biocomposites, it was around 290 ºC. According to Saska et al.[36], this event can be associated with broken hydrogen bonds to form apatites. Another feature that stands out is the high percentage of residue at the end of the test, which presented a value greater than 60% for all biocomposites produced, while for BNC it was 6.6%. These residues can be attributed to the inorganic material in the sample because the analysis was performed in an oxidizing atmosphere, which confirms the incorporation of the desired phosphate sources on the BNC membrane[36]. In this context, it is interesting to note that the higher the Cu concentration, the higher the residue, while for Mg, the behavior was the opposite, the higher the Mg concentration, the lower the residue.

### 3.3.4 Scanning Electron Microscopy (SEM)

In Figure 6A, it is possible to observe the morphology of the BNC obtained by SEM, with nanofibers randomly arranged in a three-dimensional structure, forming a highly porous structure. This type of 3D structure makes BNC an excellent biomaterial allowing the exchange of fluids containing nutrients and growth factors, as well as the extracellular matrix, stimulating cell growth. In addition, membrane porosity is essential to promote cell adhesion, initiating the process of tissue regeneration[37]. In the BNC/MgHAp biocomposites with 10%, 30% and 50% M (Figure 6B-6D), the phosphate crystals formed were in the form of plates deposited on the BNC nanofibril network but with low interaction with them. The energy scattering X-ray spectroscopy (EDS) result confirmed the presence of calcium, magnesium and phosphorus elements (Figure 6H).

According to Rabelo[38], the formation of HAp is dependent on the diffusion and adsorption of $OH^-$, $Ca^{2+}$ and $PO_4^{3-}$ ions. Thus, at more acidic pH, the adsorption of $OH^-$ ions is limited, and the most common morphological growth presents the phosphate crystals in the form of plaques. In this work, BNC was immersed in $CuCl_2$, $MgCl_2$ and $CaCl_2$ with pH between 4 and 5 and $Na_2HPO_4$ at pH 8, which may have enabled the formation of these structures.

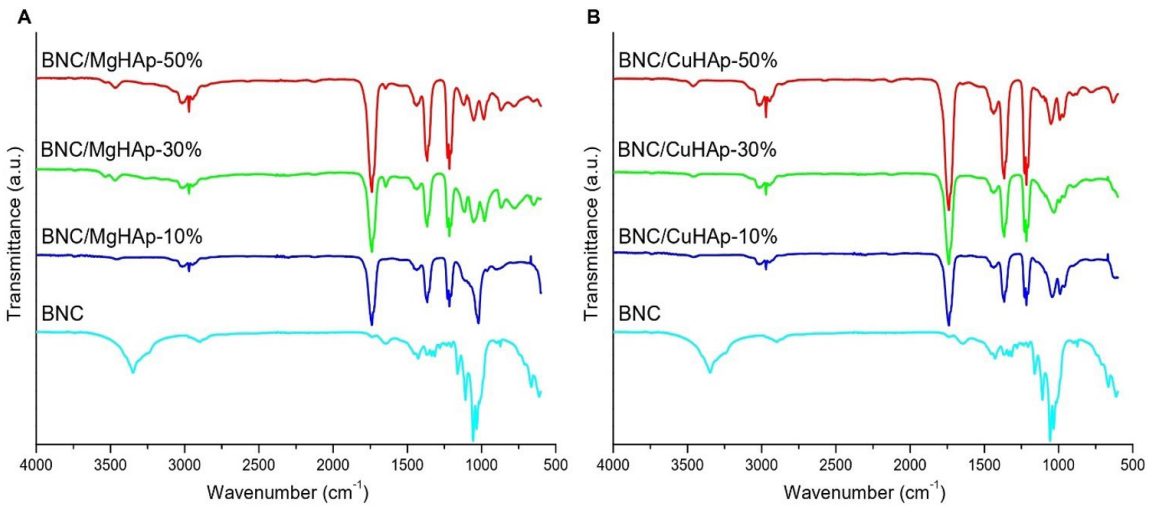


**Figure 4.** FTIR spectra obtained for BNC membranes compared with: A) BNC/MgHAp; B) BNC/CuHAp biocomposites.

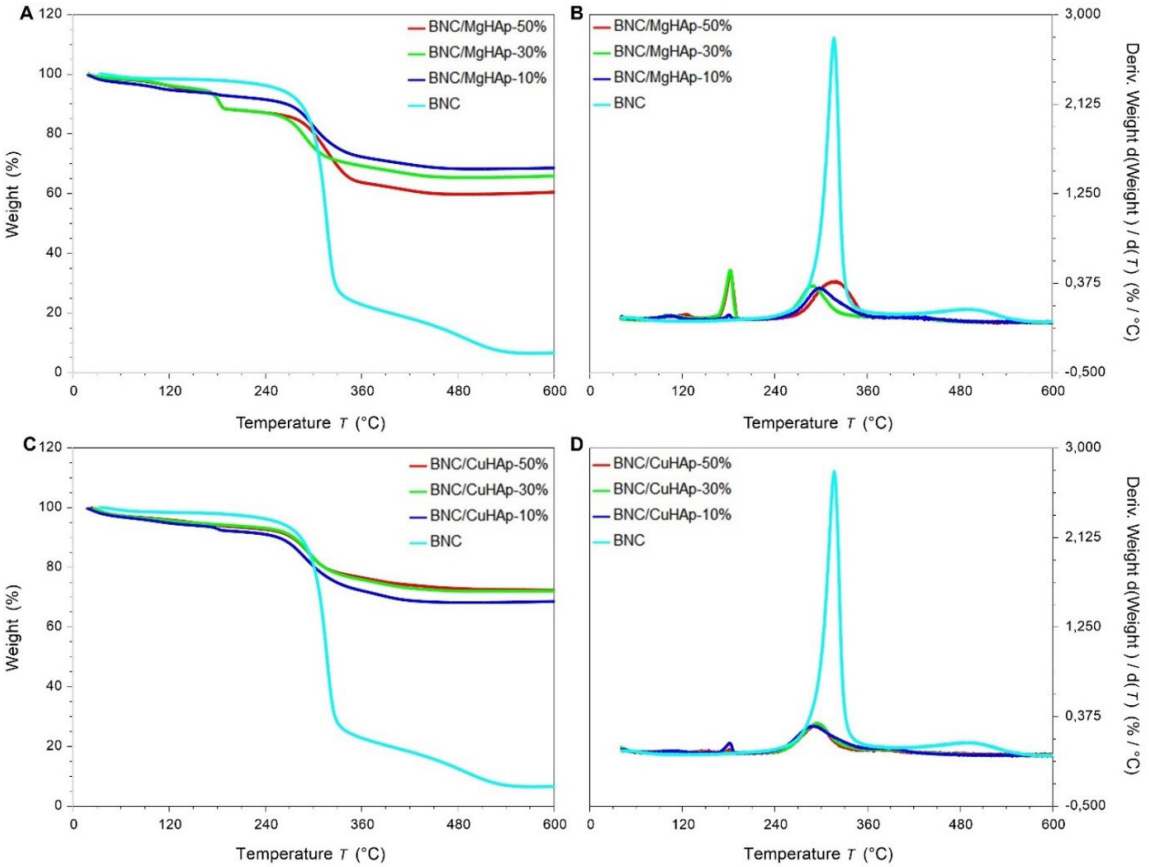


**Figure 5.** TG (A and C) and DTG (B and D) curves for BNC compared with: A,B) BNC/MgHAp; C,D) BNC/CuHAp biocomposites.

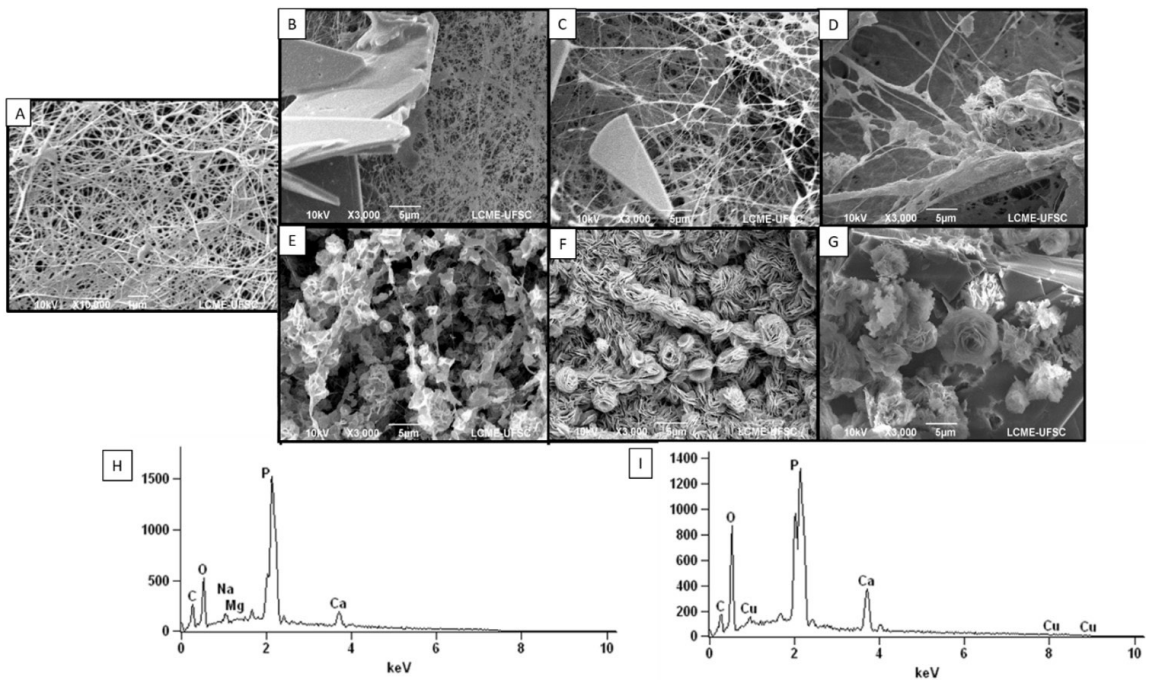


**Figure 6.** Micrographs of the surface of the membrane of BNC (A) and of the biocomposites incorporated with Mg: (B) BNC/MgHAp50%; (C) BNC/MgHAp30%; (D) BNC/MgHAp10%; (E) BNC/CuHAp 50%; (F) BNC/CuHAp 30% and (G) BNC/CuHAp 10%. The EDS of the sample surfaces are also presented in: H) BNC/MgHAp; I) BNC/CuHAp.

The morphology of the BNC/CuHAp biocomposites can be seen in Figures 6E-6G. The energy scattering X-ray spectroscopy (EDS) result also confirmed the presence of calcium, copper and phosphorus elements (Figure 6I). In Figures 6E and 6F, it is possible to observe the nanofibrils of the BNC but with the deposition of the inorganic material with lamellar crystalline form or rosettes referring to the compositions BNC/CuHAp 30% and 50%. Interestingly, in Figure 6F, the biomaterial with 30% Cu showed a denser crystalline formation, covering the entire surface of the BNC. While in the BNC/CuHAp10% sample (Figure 6G), there was a second flat crystalline form in addition to those already described as lamellar or rosettes.

Hutchens et al.[16] produced different Ca-deficient HAp BNC (CdHAp) compositions by immersion cycles. The authors observed the formation of crystallites with a needle or lamellar morphology that resembles the "rosette" structure, highlighting the similarity with the structures of apatite found in physiological bone. They found that this "rosette" structure implies that apatite was nucleated from a distinct location on the BNC nanofibrils. Moreover, at higher concentrations of CdHAp, the particles appeared to have a larger and rougher texture, indicating that the molecules of CdHAp provided secondary nucleation sites for additional apatite formation. This characteristic was also observed in Figure 6F of this work (BNC/CuAp30%). The authors observed that the distinct arrangement of the BNC nanofibers appears to have guided the growth of apatite in clusters, which can also be seen in Figures 6E and 6F. Suggesting that the apatite formed in these cases resembles native bone tissue and, through new nucleations, could stimulate bone regeneration.

### 3.4 Antimicrobial properties

Table 2 shows the result of the antimicrobial susceptibility test with the BNC/MgHAp and BNC/CuHAp biocomposites after 24 h of incubation at 30 ºC with the microorganisms *Escherichia coli* and *Staphylococcus aureus*. The absence of inhibition halos in the samples containing Mg indicates that these samples did not show an antimicrobial effect. On the other hand, all compositions of BNC/CuHAp biocomposites showed inhibition halos that varied between 11 and 13 mm in diameter (S2).

Studies reported by Demishtein et al.[39] propose that magnesium affects cell membrane permeabilization, making bacteria more sensitive. The authors present a survey of different effects on different microorganisms, further highlighting the potential to affect the formation of microbial biofilms. However, in this study, no antimicrobial effect of Mg was observed on the microorganisms tested in any of the concentrations used.

On the other hand, Cu showed higher antibacterial activity, as seen in the formation of inhibition halos for *E. coli* and *S. aureus* bacteria (Table 2 and Figure S1). Araújo et al.[7] point out that the Cu(II) ion can act on microorganisms by different mechanisms, breaking the plasma membrane, blocking biochemical pathways, forming complexes with proteins and even causing DNA damage.

### 3.5 Cytotoxicity analysis

A preliminary cytotoxicity assay is one of the critical assessments of the biological properties of biomaterials before in vivo assessment[41]. According to ISO 10993-5:2009[19], if the cell viability is greater than 70% compared to the control group, the material is considered non-cytotoxic. The cell viability results for the BNC/MgHAp and BNC/CuHAp biocomposites during the 1, 3 and 7-day incubation period are shown in Table 3.

The BNC/MgHAp biomaterials did not show change concerning the control group (BNC) after the first and third days of the test. Biocomposites containing BNC/CuHAp showed a slightly negative effect on the first analysis day, reducing cellular metabolic activity to 90% but remaining above 70%. However, after 3 days of testing, the Cu samples started to show cytotoxic effects, except for the BNC/CuHAp30% sample, which still maintained cell viability of 77.27%. However, after 7 days, all BNC/CuHAp samples confirmed a negative effect on long-term cell viability, with values around 35%.

**Table 2.** Antimicrobial activity test of the BNC/MgHAp and BNC/CuHAp biocomposites against the microorganisms *Escherichia coli* and *Staphylococcus aureus*.

| Samples | BNC | BNC/ MgHAp50% | BNC/ MgHAp30% | BNC/ MgHAp10% | BNC/ CuHAp50% | BNC/ CuHAp30% | BNC/ CuHAp10% |
|---|---|---|---|---|---|---|---|
| Ø (mm) *E. coli* | 0 | 0 | 0 | 0 | 11.5 ± 0.5 | 13.0 ± 1.0 | 11.0 ± 1.0 |
| Ø (mm) *S. aureus* | 0 | 0 | 0 | 0 | 12.5 ± 0.5 | 11.0 ± 1.0 | 11.5 ± 0.5 |

**Table 3.** Cell viability resulting from the cytotoxicity analysis of the biomaterials produced.

| Sample | 1 day | Standard deviation | 3 days | Standard deviation | 7 days | Standard deviation |
|---|---|---|---|---|---|---|
| | Cell viability (%) | | Cell viability (%) | | Cell viability (%) | |
| BNC | **100.00** | **0.02** | **100.00** | **0.02** | **100.00** | **0.18** |
| BNC/MgHAp50% | **100.27** | **0.02** | **101.72** | **0.01** | **55.41** | **0.03** |
| BNC/MgHAp30% | **100.27** | **0.02** | **103.25** | **0.02** | **100.56** | **0.15** |
| BNC/MgHAp10% | **101.47** | **0.01** | **108.32** | **0.01** | **52.46** | **0.06** |
| BNC/Cu HAp50% | **90.14** | **0.01** | **50.00** | **0.06** | **35.93** | **0.02** |
| BNC/CuHAp30% | **90.60** | **0.02** | **77.27** | **0.12** | **35.53** | **0.01** |
| BNC/CuHAp10% | **90.40** | **0.02** | **45.07** | **0.19** | **37.73** | **0.01** |

The BNC/MgHAp30% sample maintained the same behavior from the beginning to the end of the test, demonstrating that it does not have a long-term cytotoxic effect. This result makes this biomaterial the most suitable implantable material, despite not having an antimicrobial effect. The presence of $Mg^{2+}$ ions influence mineral metabolism, playing an important role in the process of bone mineralization through the activities of osteoblasts and osteoclasts[14]. Thus, the presence of Mg helps to obtain adequate mineralization in the correct formation of HAp and stimulates the production of new bone tissue. Thus, although the biomaterial BNC/MgHAp30% does not show antimicrobial activity, the partial replacement of $Ca^{2+}$ by $Mg^{2+}$ can bring other benefits for bone regeneration.

Lima et al.[40] evaluated the biocompatibility of HAp partially replaced by several divalent ions in just 1 day of contact. The authors also observed increased total viable cells in the presence of MgHAp, while CuHAp samples reduced this parameter. In the present study, however, all BNC/CuHAp samples after the first day of testing still showed 90% cell viability. Even after 3 days of testing, the sample containing 30% Cu still showed cell activity higher than 70%. However, unfortunately, in the long term, all concentrations harmed cell viability.

## 4. Conclusions

The results demonstrated a promising interaction between BNC and metallic apatites as a biocomposite for application in GBR, offering good porosity, swelling capacity and available hydroxyls to connect with HAp. These characteristics are essential in producing a biomaterial with the potential for application in GBR because they combine the osteogenic properties of HAp with the properties of BNC that make it similar to the extracellular matrix. Furthermore, the partial replacement of Ca by bivalent cations demonstrated that the effect is directly linked to the chemical nature of the ion. In this study, incorporating Cu in apatites promoted antimicrobial action against *E. coli* and *S. aureus*. However, at the tested concentrations, this element was cytotoxic in comparison, biomaterials incorporated with Mg. With particular emphasis on the BNC/MgHAp30% sample, which maintained cell viability values around 100% throughout the entire study, making this composition the most suitable for application as an implantable material and application in GBR, although not promoting antimicrobial activity. In addition, studies with multiple ionic replacements seeking synergistic effects and more remarkable similarity with natural bone composition are important factors to be investigated as future directions.

## 5. Author's Contribution

- **Conceptualization** – Michele Cristina Formolo Garcia.
- **Data curation** – Michele Cristina Formolo Garcia.
- **Formal analysis** – Michele Cristina Formolo Garcia; Giannini Pasiznick Apati.
- **Funding acquisition -** Ana Paula Testa Pezzin.
- **Investigation** – Elouise Gaulke; Michele Cristina Formolo Garcia; Bruna Segat.
- **Methodology** – Elouise Gaulke; Michele Cristina Formolo Garcia; Karina Cesca.
- **Project administration** – Ana Paula Testa Pezzin.
- **Resources** – Michele Cristina Formolo Garcia; Andréa Lima dos Santos Schneider.
- **Software** – NA.
- **Supervision** – Karina Cesca; Ana Paula Testa Pezzin; Luismar Marques Porto.
- **Validation** – Michele Cristina Formolo Garcia; Karina Cesca.
- **Visualization** – Elouise Gaulke; Michele Cristina Formolo Garcia; Bruna Segat.
- **Writing – original draft** – Elouise Gaulke; Michele Cristina Formolo Garcia.
- **Writing – review & editing** – Michele Cristina Formolo Garcia; Bruna Segat; Karina Cesca; Ana Paula Testa Pezzin.

## 6. Acknowledgements

The authors are grateful for the financial support of FAPESC and FAP/UNIVILLE for the project.

## 7. References

1. Pereira, H. F., Cengiz, I. F., Silva, F. S., Reis, R. L., & Oliveira, J. M. (2020). Scaffolds and coatings for bone regeneration. *Journal of Materials Science. Materials in Medicine*, *31*(3), 27. http://dx.doi.org/10.1007/s10856-020-06364-y. PMid:32124052.
2. Zou, L., Zhang, Y., Liu, X., Chen, J., & Zhang, Q. (2019). Biomimetic mineralization on natural and synthetic polymers to prepare hybrid scaffolds for bone tissue engineering. *Colloids and Surfaces. B, Biointerfaces*, *178*, 222-229. http://dx.doi.org/10.1016/j.colsurfb.2019.03.004. PMid:30870789.
3. Filippi, M., Born, G., Chaaban, M., & Scherberich, A. (2020). Natural polymeric scaffolds in bone regeneration. *Frontiers in Bioengineering and Biotechnology*, *8*, 474. http://dx.doi.org/10.3389/fbioe.2020.00474. PMid:32509754.
4. Luz, E. P. C. G., Borges, M. F., Andrade, F. K., Rosa, M. F., Infantes-Molina, A., Rodríguez-Castellón, E., & Vieira, R. S. (2018). Strontium delivery systems based on bacterial cellulose and hydroxyapatite for guided bone regeneration. *Cellulose*, *25*(11), 6661-6679. http://dx.doi.org/10.1007/s10570-018-2008-8.
5. Shi, R., Huang, Y. H., Ma, C., Wu, C., & Tian, W. (2019). Current advances for bone regeneration based on tissue engineering strategies. *Frontiers of Medicine*, *13*(2), 160-188. http://dx.doi.org/10.1007/s11684-018-0629-9. PMid:30047029.
6. Ryngajłło, M., Kubiak, K., Jędrzejczak-Krzepkowska, M., Jacek, P., & Bielecki, S. (2019). Comparative genomics of the Komagataeibacter strains: efficient bionanocellulose producers. *MicrobiologyOpen*, *8*(5), e00731. http://dx.doi.org/10.1002/mbo3.731. PMid:30365246.
7. Araújo, I. M. S., Silva, R. R., Pacheco, G., Lustri, W. R., Tercjak, A., Gutierrez, J., Souza, J. R. Jr., Azevedo, F. H. C., Figuêredo, G. S., Vega, M. L., Ribeiro, S. J. L., & Barud, H. S. (2018). Hydrothermal synthesis of bacterial cellulose–copper oxide nanocomposites and evaluation of their antimicrobial activity. *Carbohydrate Polymers*, *179*, 341-349. http://dx.doi.org/10.1016/j.carbpol.2017.09.081. PMid:29111060.
8. Pang, M., Huang, Y., Meng, F., Zhuang, Y., Liu, H., Du, M., Ma, Q., Wang, Q., Chen, Z., Chen, L., Cai, T., & Cai, Y.

(2020). Application of bacterial cellulose in skin and bone tissue engineering. *European Polymer Journal*, *122*, 109365. http://dx.doi.org/10.1016/j.eurpolymj.2019.109365.

9. Maia, M. T., Luz, É. P. C. G., Andrade, F. K., Rosa, M. F., Borges, M. F., Arcanjo, M. R. A., & Vieira, R. S. (2021). Advances in bacterial cellulose/strontium apatite composites for bone applications. *Polymer Reviews*, *61*(4), 736-764. http://dx.doi.org/10.1080/15583724.2021.1896543.
10. Chocholata, P., Kulda, V., & Babuska, V. (2019). Fabrication of scaffolds for bone-tissue regeneration. *Materials*, *12*(4), 568. http://dx.doi.org/10.3390/ma12040568. PMid:30769821.
11. Hidalgo-Robatto, B. M., López-Álvarez, M., Azevedo, A. S., Dorado, J., Serra, J., Azevedo, N. F., & González, P. (2018). Pulsed laser deposition of copper and zinc doped hydroxyapatite coatings for biomedical applications. *Surface and Coatings Technology*, *333*, 168-177. http://dx.doi.org/10.1016/j.surfcoat.2017.11.006.
12. Gopi, D., Shinyjoy, E., & Kavitha, L. (2014). Synthesis and spectral characterization of silver/magnesium co-substituted hydroxyapatite for biomedical applications. *Spectrochimica Acta. Part A: Molecular and Biomolecular Spectroscopy*, *127*, 286-291. http://dx.doi.org/10.1016/j.saa.2014.02.057. PMid:24632237.
13. Xu, T., He, X., Chen, Z., He, L., Lu, M., Ge, J., Weng, J., Mu, Y., & Duan, K. (2019). Effect of magnesium particle fraction on osteoinduction of hydroxyapatite sphere-based scaffolds. *Journal of Materials Chemistry. B, Materials for Biology and Medicine*, *7*(37), 5648-5660. http://dx.doi.org/10.1039/C9TB01162E. PMid:31465084.
14. Predoi, D., Iconaru, S. L., Predoi, M. V., Stan, G. E., & Buton, N. (2019). Synthesis, characterization, and antimicrobial activity of magnesium-doped hydroxyapatite suspensions. *Nanomaterials*, *9*(9), 1295. http://dx.doi.org/10.3390/nano9091295. PMid:31514280.
15. Vranceanu, D. M., Ionescu, I. C., Ungureanu, E., Cojocaru, M. O., Vladescu, A., & Cotrut, C. M. (2020). Magnesium doped hydroxyapatite-based coatings obtained by pulsed galvanostatic electrochemical deposition with adjustable electrochemical behavior. *Coatings*, *10*(8), 727. http://dx.doi.org/10.3390/coatings10080727.
16. Hutchens, S. A., Benson, R. S., Evans, B. R., O'Neill, H. M., & Rawn, C. J. (2006). Biomimetic synthesis of calcium-deficient hydroxyapatite in a natural hydrogel. *Biomaterials*, *27*(26), 4661-4670. http://dx.doi.org/10.1016/j.biomaterials.2006.04.032. PMid:16713623.
17. Zeng, X., & Ruckenstein, E. (1996). Control of pore sizes in macroporous chitosan and chitin membranes. *Industrial & Engineering Chemistry Research*, *35*(11), 4169-4175. http://dx.doi.org/10.1021/ie960270j.
18. Bauer, A. W., Kirby, W. M., Sherris, J. C., & Turck, M. (1966). Antibiotic susceptibility testing by a standardized single disk method. *American Journal of Clinical Pathology*, *45*(4_ts), 493-496. http://dx.doi.org/10.1093/ajcp/45.4_ts.493. PMid:5325707.
19. International Organization for Standardization – ISO. (2009). *ISO/EN10993-5: biological evaluation of medical devices - part 5: tests for in vitro cytotoxicity*. Geneva: ISO.
20. Aguilar, A. E. M., Fagundes, A. P., Macuvele, D. L. P., Cesca, K., Porto, L., Padoin, N., Soares, C., & Riella, H. G. (2021). Green synthesis of nano hydroxyapatite: morphology variation and its effect on cytotoxicity against fibroblast. *Materials Letters*, *284*(Part 2), 129013. http://dx.doi.org/10.1016/j.matlet.2020.129013.
21. Kim, H.-L., Jung, G.-Y., Yoon, J.-H., Han, J.-S., Park, Y.-J., Kim, D.-G., Zhang, M., & Kim, D.-J. (2015). Preparation and characterization of nano-sized hydroxyapatite/alginate/chitosan composite scaffolds for bone tissue engineering. *Materials Science and Engineering C*, *54*, 20-25. http://dx.doi.org/10.1016/j.msec.2015.04.033. PMid:26046263.
22. Jin, H.-H., Kim, D.-H., Kim, T.-W., Shin, K.-K., Jung, J. S., Park, H.-C., & Yoon, S.-Y. (2012). In vivo evaluation of porous hydroxyapatite/chitosan–alginate composite scaffolds for bone tissue engineering. *International Journal of Biological Macromolecules*, *51*(5), 1079-1085. http://dx.doi.org/10.1016/j.ijbiomac.2012.08.027. PMid:22959955.
23. Salim, S. A., Loutfy, S. A., El-Fakharany, E. M., Taha, T. H., Hussien, Y., & Kamoun, E. A. (2021). Influence of chitosan and hydroxyapatite incorporation on properties of electrospun PVA/HA nanofibrous mats for bone tissue regeneration: nanofibers optimization and in-vitro assessment. *Journal of Drug Delivery Science and Technology*, *62*, 102417. http://dx.doi.org/10.1016/j.jddst.2021.102417.
24. Lakrat, M., Jodati, H., Mejdoubi, E. M., & Evis, Z. (2023). Synthesis and characterization of pure and Mg, Cu, Ag, and Sr doped calcium-deficient hydroxyapatite from brushite as precursor using the dissolution-precipitation method. *Powder Technology*, *413*, 118026. http://dx.doi.org/10.1016/j.powtec.2022.118026.
25. He, M., Chang, C., Peng, N., & Zhang, L. (2012). Structure and properties of hydroxyapatite/cellulose nanocomposite films. *Carbohydrate Polymers*, *87*(4), 2512-2518. http://dx.doi.org/10.1016/j.carbpol.2011.11.029.
26. An, S.-J., Lee, S.-H., Huh, J.-B., Jeong, S. I., Park, J.-S., Gwon, H.-J., Kang, E.-S., Jeong, C.-M., & Lim, Y.-M. (2017). Preparation and characterization of resorbable bacterial cellulose membranes treated by electron beam irradiation for guided bone regeneration. *International Journal of Molecular Sciences*, *18*(11), 2236. http://dx.doi.org/10.3390/ijms18112236. PMid:29068426.
27. Huang, Y., Wang, J., Yang, F., Shao, Y., Zhang, X., & Dai, K. (2017). Modification and evaluation of micro-nano structured porous bacterial cellulose scaffold for bone tissue engineering. *Materials Science and Engineering C*, *75*, 1034-1041. http://dx.doi.org/10.1016/j.msec.2017.02.174. PMid:28415386.
28. Salarian, M., Solati-Hishjin, M., Sara Shafiei, S., Goudarzi, A., Salarian, R., & Nemati, A. (2009). Surfactant-assisted synthesis and characterization of hydroxyapatite nanorods under hydrothermal conditions. *Materials Science Poland*, *27*(4), 961-971. Retrieved in 2023, August 18, from https://materialsscience.pwr.edu.pl/bi/vol27no4/articles/ms_03_2008_204sala.pdf
29. Panda, S., Behera, B. P., Bhutia, S. K., Biswas, C. K., & Paul, S. (2022). Rare transition metal doped hydroxyapatite coating prepared via microwave irradiation improved corrosion resistance, biocompatibility and anti-biofilm property of titanium alloy. *Journal of Alloys and Compounds*, *918*, 165662. http://dx.doi.org/10.1016/j.jallcom.2022.165662.
30. Minatti, T. C. D. S. (2020). *Nanocompósito celulose bacteriana e hidroxiapatita para remoção de zinco de efluentes industriais* (Master's dissertation). Universidade Federal de Santa Catarina, Joinville.
31. Huang, Y., Zhang, X., Zhao, R., Mao, H., Yan, Y., & Pang, X. (2015). Antibacterial efficacy, corrosion resistance, and cytotoxicity studies of copper-substituted carbonated hydroxyapatite coating on titanium substrate. *Journal of Materials Science*, *50*(4), 1688-1700. http://dx.doi.org/10.1007/s10853-014-8730-1.
32. Favi, P. M., Ospina, S. P., Kachole, M., Gao, M., Atehortua, L., & Webster, T. J. (2016). Preparation and characterization of biodegradable nano hydroxyapatite–bacterial cellulose composites with well-defined honeycomb pore arrays for bone tissue engineering applications. *Cellulose*, *23*(2), 1263-1282. http://dx.doi.org/10.1007/s10570-016-0867-4.

33. Wan, Y., Zuo, G., Yu, F., Huang, Y., Ren, K., & Luo, H. (2011). Preparation and mineralization of three-dimensional carbon nanofibers from bacterial cellulose as potential scaffolds for bone tissue engineering. *Surface and Coatings Technology*, *205*(8-9), 2938-2946. http://dx.doi.org/10.1016/j.surfcoat.2010.11.006.
34. Lima, L. R., Santos, D. B., Santos, M. V., Barud, H. S., Henrique, M. A., Pasquini, D., Pecoraro, E., & Ribeiro, S. J. L. (2015). Nanocristais de celulose a partir de celulose bacteriana. *Química Nova*, *38*(9), 1140-1147. http://dx.doi.org/10.5935/0100-4042.20150131.
35. Tõnsuaadu, K., Gross, K. A., Pluduma, L., & Veiderma, M. (2012). A review on the thermal stability of calcium apatites. *Journal of Thermal Analysis and Calorimetry*, *110*(2), 647-659. http://dx.doi.org/10.1007/s10973-011-1877-y.
36. Saska, S., Barud, H. S., Gaspar, A. M. M., Marchetto, R., Ribeiro, S. J. L., & Messaddeq, Y. (2011). Bacterial cellulose-hydroxyapatite nanocomposites for bone regeneration. *International Journal of Biomaterials*, *2011*, 175362. http://dx.doi.org/10.1155/2011/175362. PMid:21961004.
37. Robbins, M., Pisupati, V., Azzarelli, R., Nehme, S. I., Barker, R. A., Fruk, L., & Schierle, G. S. K. (2021). Biofunctionalised bacterial cellulose scaffold supports the patterning and expansion of human embryonic stem cell-derived dopaminergic progenitor cells. *Stem Cell Research & Therapy*, *12*(1), 574. http://dx.doi.org/10.1186/s13287-021-02639-5. PMid:34774094.
38. Rabelo, J. S. No. (2015). *Efeitos da substituição iônica por estrôncio na morfologia de cristais de fosfatos de cálcio e no polimorfismo da hidroxiapatita hexagonal e monoclínica* (Doctoral thesis). Universidade Federal de Santa Catarina, Florianópolis.
39. Demishtein, K., Reifen, R., & Shemesh, M. (2019). Antimicrobial properties of magnesium open opportunities to develop healthier food. *Nutrients*, *11*(10), 2363. http://dx.doi.org/10.3390/nu11102363. PMid:31623397.
40. Lima, I. R., Alves, G. G., Soriano, C. A., Campaneli, A. P., Gasparoto, T. H., Ramos, E. S. Jr., Sena, L. Á., Rossi, A. M., & Granjeiro, J. M. (2011). Understanding the impact of divalent cation substitution on hydroxyapatite: an in vitro multiparametric study on biocompatibility. *Journal of Biomedical Materials Research. Part A*, *98A*(3), 351-358. http://dx.doi.org/10.1002/jbm.a.33126. PMid:21626666.
41. Lin, B., Zhong, M., Zheng, C., Cao, L., Wang, D., Wang, L., Liang, J., & Cao, B. (2015). Preparation and characterization of dopamine-induced biomimetic hydroxyapatite coatings on the AZ31 magnesium alloy. *Surface and Coatings Technology*, *281*, 82-88. http://dx.doi.org/10.1016/j.surfcoat.2015.09.033.

*Received: Jan. 10, 2023*
*Revised: Jul. 18, 2023*
*Accepted: Aug. 18, 2023*

## Supplementary Material

Supplementary material accompanies this paper.

Table S1. Maximum degradation temperature (Tpeak) and percentage of mass loss (M%) data, obtained from the TG and DTG curves of BNC (standard) and BNC/CuHAp and BNC/MgHAp samples.

Figure S1. Antimicrobial susceptibility test of the BNC/MgHAp and BNC/CuHAp biocomposites against the microorganisms Escherichia coli and Staphylococcus aureus.

This material is available as part of the online article from https://doi.org/10.1590/0104-1428.20220121

Polímeros
ISSN 1678-5169 (Online)

https://doi.org/10.1590/0104-1428.20220121

ORIGINAL ARTICLE

# Evaluation of potential biomaterials for application in guide bone regeneration from Bacterial Nanocellulose/Hydroxyapatite

**Elouise Gaulke[1], Michele Cristina Formolo Garcia[2,3]*, Bruna Segat[2], Giannini Pasiznick Apati[2], Andréa Lima dos Santos Schneider[2,3], Ana Paula Testa Pezzin[1], Karina Cesca[4] and Luismar Marques Porto[4]**

*[1]Laboratório de Materiais, Programa de Pós-graduação em Engenharia de Processos, Universidade da Região de Joinville, Joinville, SC, Brasil*

*[2]Laboratório de Biotecnologia I, Departamento de Engenharia Química, Universidade da Região de Joinville, Joinville, SC, Brasil*

*[3]Laboratório de Biotecnologia I, Programa de Pós-graduação em Saúde e Meio Ambiente, Universidade da Região de Joinville, Joinville, SC, Brasil*

*[4]Laboratório de Engenharia Biológica, Programa de Pós-graduação em Engenharia Química, Universidade Federal de Santa Catarina, Florianópolis, SC, Brasil*

**micheleformologarcia@gmail.com*

## Supplementary Material

**Table S1.** Maximum degradation temperature (Tpeak) and percentage of mass loss (M%) data, obtained from the TG and DTG curves of BNC (standard) and BNC/CuHAp and BNC/MgHAp samples.

| Sample | $M_1$ (%) | $M_2$ (%) | $T_{peak2}$ (°C) | $M_3$ (%) | $T_{peak3}$ (°C) | $M_4$ (%) | $T_{peak4}$ (°C) | Residue (%) |
|---|---|---|---|---|---|---|---|---|
| BNC | 1.8 | - | - | 74.4 | 316.5 | 17.2 | 493.9 | 6.58 |
| BNC/MgHAp50% | 5.3 | 6.6 | 182.4 | 23.6 | 316.4 | 4.4 | 368.4 | 60.45 |
| BNC/MgHAp30% | 4.8 | 7.1 | 181.6 | 17.8 | 288.7 | 4.7 | 473.9 | 65.91 |
| BNC/MgHAp10% | 5.9 | 1.6 | 180.5 | 19.5 | 297.9 | 4.7 | 374.1 | 68.58 |
| BNC/CuHAp 50% | 4.0 | - | - | 16.9 | 294.7 | 5.6 | 417.4 | 72.33 |
| BNC/CuHAp 30% | 5.2 | - | - | 16.9 | 294.0 | 5.8 | 354.1 | 72.01 |
| BNC/CuHAp 10% | 5.9 | 2.0 | 180.4 | 17.3 | 288.1 | 6.5 | 394.0 | 68.56 |

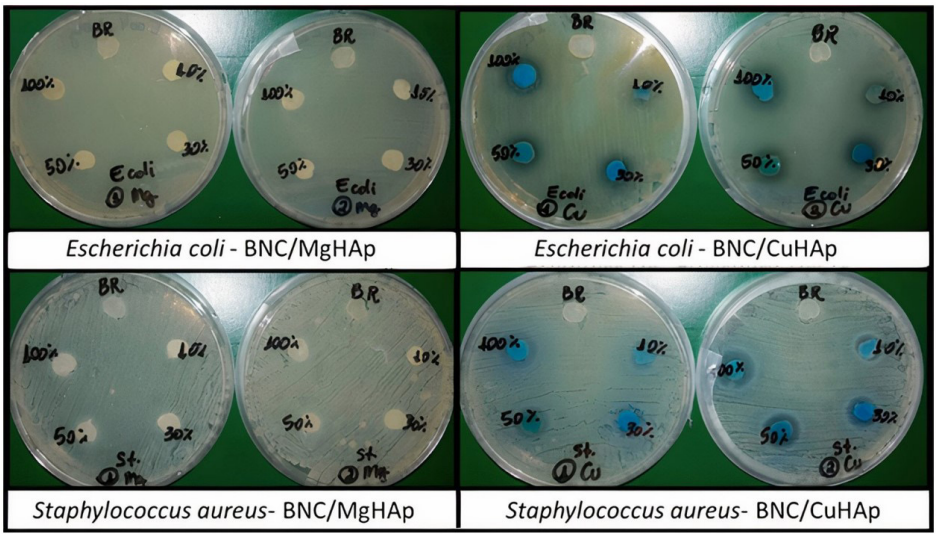


**Figure S1.** Antimicrobial susceptibility test of the BNC/MgHAp and BNC/CuHAp biocomposites against the microorganisms *Escherichia coli* and *Staphylococcus aureus*.